https://doi.org/10.5194/egusphere-2025-4172
Preprint. Discussion started: 4 September 2025

A Robust Variational Framework for Cyclogeostrophic Ocean Surface Current Retrieval

Vadim Bertrand[1], Julien Le Sommer[1], Victor Vianna Zaia De Almeida[1], Adeline Samson[2], and Emmanuel Cosme[1]

[1]Univ. Grenoble Alpes, CNRS, IRD, Grenoble INP, IGE, Grenoble, F-38000, France
[2]Univ. Grenoble Alpes, CNRS, Grenoble INP, LJK, Grenoble, F-38000, France

Correspondence: Vadim Bertrand (vadim.bertrand@univ-grenoble-alpes.fr)

Abstract. Estimations of surface currents at submesoscales (1–50 km) are crucial for operational applications and environmental monitoring, yet accurately deriving them from satellite observations remains a challenge. While the geostrophic approximation has long been used to infer ocean surface currents from Sea Surface Height (SSH), it neglects nonlinear advection, which can become significant at submesoscales. To address this limitation, we present a robust and efficient variational method for inverting the cyclogeostrophic balance equation, implemented in the open-source Python library `jaxparrow`. Unlike the traditional iterative approaches, our method reformulates the inversion as an optimization problem, providing stable estimates even in regions where a cyclogeostrophic solution may not exist. Using both DUACS and the high-resolution NeurOST SSH products, we demonstrate that cyclogeostrophic corrections become increasingly relevant at finer spatial scales. Validation against drifter-derived velocities shows that our approach consistently improves current estimates in energetic regions, reducing errors by up to 20 % compared to geostrophy alone in energetic regions of the global ocean. These results support the systematic inclusion of cyclogeostrophic inversion in the analysis of high-resolution SSH fields.

1 Introduction

Surface ocean currents play a critical role in a wide range of environmental and operational processes (Röhrs et al., 2023). At spatial scales from 1 to 50 km—commonly referred to as submesoscales—these currents influence the exchange of energy between the ocean and atmosphere, with important implications for climate studies (Hewitt et al., 2022). They are also essential for numerous practical applications, including offshore operations, renewable energy development (Ferreira et al., 2016), and the forecasting of object trajectories in the ocean. Accurate surface current information supports search-and-rescue missions, iceberg tracking, and the management of marine debris and oil spills (Breivik et al., 2013; Keghouche et al., 2009; Trinanes et al., 2016; De Dominicis et al., 2016). Additionally, submesoscale dynamics contribute to vertical mixing in the upper ocean, affecting biological productivity and the transport of nutrients and plankton, which are key components of marine ecosystems (Mahadevan, 2016; Lévy et al., 2018).

https://doi.org/10.5194/egusphere-2025-4172
Preprint. Discussion started: 4 September 2025

Satellite observations of Sea Surface Height (SSH) and Sea Surface Temperature (SST) both provide valuable insights into surface currents and fine-scale ocean dynamics. Since the 90's, satellite altimetry has provided SSH observations that are then processed into global gridded maps (Le Traon and Dibarboure, 1999) from which geostrophic velocities can be derived (Le Traon and Dibarboure, 2002). The effective resolution of these maps are estimated at nearly 200 km at mid-latitudes (Taburet et al., 2019), keeping the submesoscale spectrum invisible to us. The Surface Water and Ocean Topography mission (SWOT, Fu, 2008; Fu et al., 2012), launched in 2022, has been designed to increase the spatial resolution of earlier altimeters and reach 15 km of effective resolution in the satellite swath (Morrow et al., 2019; Nencioli et al., 2025; Wang et al., 2025). Complementary to altimetry, SST provides high-resolution snapshots of ocean surface structures, revealing submesoscale features which are not observed by conventional altimeters. Many research efforts are presently under way to derive global maps of SSH and currents with a resolution that would enable the observation of the upper spectrum of the mesoscale dynamics by synthesizing classical altimetry with SWOT (Le Guillou et al., 2021; Ubelmann et al., 2021; Ballarotta et al., 2023; Le Guillou et al., 2023; Xiao et al., 2023) and/or SST (Buongiorno Nardelli et al., 2022; Archambault et al., 2023; Fablet et al., 2024; Le Guillou et al., 2024; Martin et al., 2024).

Under some dynamical conditions, accurately deriving ocean surface currents from high-resolution SSH images or maps requires using the cyclogeostrophic balance approximation rather than the usual geostrophic approximation. The cyclogeostrophic balance equation mathematically describes the balance between the pressure gradient force, the Coriolis force (these two only making the geostrophic balance), and the convective force:

$$(\boldsymbol{u}_{cg} \cdot \nabla)\boldsymbol{u}_{cg} + f\boldsymbol{k} \wedge \boldsymbol{u}_{cg} = -g\nabla\eta \tag{1}$$

where $\boldsymbol{u}_{cg}$ is the horizontal, cyclogeostrophic velocity, f the Coriolis parameter, g the gravity, η the SSH, $\boldsymbol{k}$ the vertical unit vector. Bold fonts indicate vectors. This equation extends the usual geostrophic balance equation when the Rossby number Ro, defined as the ratio between the scales of the convective force and the Coriolis force, approaches 1. This "$Ro \approx 1$" regime actually characterizes the submesoscale regime (McWilliams, 2019; Taylor and Thompson, 2023). Cyclogeostrophic currents can significantly differ from geostrophic currents in some regions such as the Mozambique channel (Penven et al., 2014) or the Mediterranean sea (Ioannou et al., 2019). A global assessment has been performed by Cao et al. (2023) and leads to a similar conclusion.

Several methods to solve the cyclogeostrophic inverse problem have been proposed in the past literature but they all exhibit drawbacks, and publicly available, well maintained implementations are missing. Penven et al. (2014) provides a review of these methods. The most widely employed, proposed by Arnason et al. (1962) and Endlich (1961), is iterative. Unfortunately, Arnason's study shows it can be unstable. This has been confirmed by several authors later (Penven et al., 2014; Ioannou et al., 2019). In particular, the method is not suitable when the cyclogerostrophic equation has no solution. Further details are given in Sect. 2.

https://doi.org/10.5194/egusphere-2025-4172
Preprint. Discussion started: 4 September 2025

This paper proposes a new and modern numerical solution for the cyclogeostrophic inverse problem. The first novelty lies in the mathematical formulation of the problem, in a variational form. The second novelty lies in the use of the `JAX` Python library to solve the optimization problem numerically. These developments make a new, open-source, and numerically efficient Python package for the cyclogeostrophic inversion, named `jaxparrow`. The variational resolution corrects the shortcomings of the historical iterative method and enables a quantification of the impact of cyclogeostrophic corrections as effective resolution of SSH fields increases.

The paper is structured as follows: Section 2 reviews Arnason's iterative method for the cyclogeostrophic inversion, describes the new variational method, and its implementation with `JAX`. Section 3 details the data used and the experimental setup of our study. Section 4 presents global applications with operational SSH maps: DUACS, available through the Copernicus Marine Environment Monitoring Service (CMEMS); and NeurOST, available through the Physical Oceanography Distributed Active Archive Center (PODAAC). For both products assessments of the derived currents using drifters are included.

2 Resolution of the cyclogeostrophic inversion problem

This section presents methods used to solve the cyclogeostrophic inversion problem. We first review the historical iterative approach proposed by Arnason et al. (1962), which has been widely used despite known limitations. We then introduce a novel variational formulation of the inversion problem that addresses some of these shortcomings. Finally, we describe our practical implementation of this variational approach using modern automatic differentiation tools.

2.1 State of the art: Arnason's (1962) iterative method

The vector product of $\mathbf{k}$ with Eq. 1, denotating $\boldsymbol{u}_g$ the geostrophic velocity, leads to:

$$\boldsymbol{u}_{cg} - \frac{\boldsymbol{k}}{f} \wedge (\boldsymbol{u}_{cg} \cdot \nabla)\boldsymbol{u}_{cg} = \boldsymbol{u}_g \tag{2}$$

Then the iterations proposed by Arnason et al. (1962) to get the cyclogeostrophic velocity are initialized with $\boldsymbol{u}_{cg}^{(0)} = \boldsymbol{u}_g$ and implement:

$$\boldsymbol{u}_{cg}^{(n+1)} = \boldsymbol{u}_g + \frac{\boldsymbol{k}}{f} \wedge (\boldsymbol{u}_{cg}^{(n)} \cdot \nabla)\boldsymbol{u}_{cg}^{(n)} \tag{3}$$

As initially mentioned by Arnason et al. (1962), these iterations do not always converge; an *ad hoc* and imperfect stopping strategy is generally implemented to avoid their divergence. A typical case of divergence is when the cyclogeostrophic equation has no solution, which happens in some circumstances (Ioannou et al., 2019). Penven et al. (2014) stops the iterations at any grid point i when the residual $|\boldsymbol{u}_{cg,i}^{(n+1)} - \boldsymbol{u}_{cg,i}^{(n)}|$ falls below 0.01 or starts to increase. Ioannou et al. (2019) implements this with two additional ingredients: the initial geostrophic velocity field is projected, with a cubic interpolation, on a grid 3 times finer than the initial one. This is to "improve the computation of the velocity derivatives" in Eq. 3. The second modification is in the calculation of the residual norm for each grid point, which includes now the 8 neighboring grid points. From our own

https://doi.org/10.5194/egusphere-2025-4172
Preprint. Discussion started: 4 September 2025

experience, illustrated in Figures 2 and A1, this iteration-stopping strategy can sometimes lead to noisy or unrealistic velocity fields. Thus there is a need for an alternate approach.

2.2 Variational formulation

We recast the cyclogeostrophic inversion problem in a variational form, by searching for the velocity field $\boldsymbol{u}_{cg}$ that minimizes the following loss function:

$$J(\boldsymbol{u}_{cg}) = \int_{\Omega} [\Delta_{cg}(\boldsymbol{u}_{cg}(\boldsymbol{x}))]^2 d\boldsymbol{x} \tag{4}$$

where Ω is the 2D spatial domain and Δ_{cg} denotes the *cyclogeostrophic imbalance* computed locally at each point $\boldsymbol{x} = (x, y)$ in the discretized domain:

$$\Delta_{cg}(\boldsymbol{u}_{cg}) = \left\| \boldsymbol{u}_{cg} - \frac{\boldsymbol{k}}{f} \wedge (\boldsymbol{u}_{cg} \cdot \nabla)\boldsymbol{u}_{cg} - \boldsymbol{u}_g \right\| \tag{5}$$

where $\|\cdot\|$ is the L_2 norm for a 2-component velocity vector: $\|\boldsymbol{u}(\boldsymbol{x})\| = \sqrt{u(\boldsymbol{x})^2 + v(\boldsymbol{x})^2}$, using the standard notations for the zonal and meridional velocities. In Eq. 4, we make it explicit that the loss function is the domain integral of a locally computed norm (the integration could be hidden in the norm operator) in anticipation of further discussions.

The variational formulation is expected to solve the divergence problem of the iterative method; it also provides a measure of the deviation from the cyclogeostrophic solution (when it exists). Where the cyclogeostrophic imbalance Δ_{cg} reaches 0, the solution is the cyclogeostrophic velocity. And where there is no cyclogeostrophic solution, the minimum of J yields a smooth velocity field that does not exhibit the unrealistic features yielded by the iterative method. Interestingly, the cyclogeostrophic imbalance is a straightforward indication of where a cyclogeostrophic velocity can be found, and where it cannot. It is not possible to determine the physical nature of the velocity solution when Δ_{cg} does not reach 0. But it is still possible to quantify a deviation from the cyclogeostrophic equilibrium.

2.3 Implementation

Our cyclogeostrophic inversion library, `jaxparrow` (Bertrand et al., 2025), is implemented with `JAX` (Bradbury et al., 2018), a Python library developed by Google to perform two main operations on Python functions: acceleration and automatic differentiation. `jaxparrow` leverages both features. The automatic differentiation capability directly provides the gradient of J, which can be used for gradient-based minimization methods. For the minimization itself, `jaxparrow` implements `Optax` (DeepMind et al., 2020), a gradient processing and optimization library specifically developed for `JAX`.

`jaxparrow` handles gridded data, making it well-suited for estimating cyclogeostrophic currents from SSH derived from models, Level-4 products, and also 2D Level-3 products as illustrated in Fig. B1. In `jaxparrow`, the partial derivatives are computed using finite differences on Arakawa C-grids.

To support further evaluation of our variational method and facilitate the integration of cyclogeostrophic currents into a global operational product, our library is easily installable via `pip`, with its code publicly available on GitHub.

https://doi.org/10.5194/egusphere-2025-4172
Preprint. Discussion started: 4 September 2025

3 Data and experimental setup

This section describes the data sources and methodology used to assess cyclogeostrophic surface current reconstructions. We first present the input satellite SSH products and the drifter dataset used for validation. We then detail the experimental setup, including the computation of derived kinematic fields and the evaluation procedure based on drifter-derived velocities.

3.1 Input and validation data

3.1.1 Operational SSH products

As Penven et al. (2014); Ioannou et al. (2019); Cao et al. (2023), we use the standard Data Unification and Altimeter Combination System (DUACS, 2024) SSH global product. In its most recent version, DUACS provides data with daily temporal resolution on a grid with a spatial resolution of 1/8°. As reported by Ballarotta et al. (2019), DUACS effective resolution (computed using the Signal to Noise Ratio method) ranges globally from 100 km at high latitudes to 800 km in the equatorial band.

To illustrate the relevance of cyclogeostrophic corrections as effective resolution increases, we also use the newer experimental global product NeurOST (NeurOST, 2024). NeurOST gridded data has a temporal resolution of one day and a spatial resolution of 1/10°. Martin et al. (2024) shows that by combining satellite observations of SSH and SST, NeurOST improves the effective resolution by up to 30 % compared to DUACS, particularly in the Gulf Stream region, where NeurOST achieves an effective resolution of 108 km versus 150 km for DUACS.

The present study covers the period from 2010 to 2022 (inclusive), corresponding to the availability period of both DUACS and NeurOST products.

3.1.2 Global Drifter Program (GDP) dataset

We used 6-hourly interpolated surface current velocity measurements from drifters, collected in the GDP database (Lumpkin and Centurioni, 2019). The GDP database includes data from drifters of various types and shapes with differing sensitivities to wind. To ensure that the reference velocities are not influenced by direct wind forcing on the drifters, we restricted our analysis to drogued SVP-type drifters. At the global scale, over the period 2010—2022, it represents approximately 9.8 million observations from around 12,500 drifters.

3.2 Experimental setup

3.2.1 Derived kinematics

Starting from global SSH maps, we present several diagnostics to assess the impact of accurately computed cyclogeostrophic velocities. Due to the use of Arakawa C-grids, variables must be carefully interpolated as needed when performing numerical computations.

https://doi.org/10.5194/egusphere-2025-4172
Preprint. Discussion started: 4 September 2025

We compute the cyclogeostrophic imbalance from Eq. 5 and use it as a local measure of deviation from cyclogeostrophy, expressed in ms^{-1}. To better highlight divergences while estimating cyclogeostrophic currents, spatial deviations from cyclogeostrophy are aggregated over time by taking the maximum of the 7-days moving average, following the approach of Fig. 12 in Ioannou et al. (2019).

We derive geostrophic and cyclogeostrophic velocities from SSH using `jaxparrow`. Iterative cyclogeostrophic velocities are computed using Eq. 3, with the stopping procedure described in Sec. 2.1 (same as Penven et al., 2014; Cao et al., 2023). Variational cyclogeostrophic velocities are estimated by minimizing J from Eq. 4 using gradient descent with a fixed learning rate of 5×10^{-3} for 2,000 iterations, using geostrophic velocities as the initial guess.

Relative vorticity provides insight into ocean dynamics and the quality of reconstructed current velocities. It represents the spinning motion of a water parcel relative to the Earth and is defined as the curl of the velocity:

$$\zeta = \frac{\partial v}{\partial x} - \frac{\partial u}{\partial y} \tag{6}$$

Since it requires computing spatial derivatives, it is expected to highlight noise in velocity fields. Relative vorticity maps are also computed using `jaxparrow`.

Eddy Kinetic Energy (EKE) quantifies the kinetic energy associated with the time-varying component of the flow and as such is a good indicator of the mesoscale dynamics. Following Cao et al. (2023) we compute it as:

$$\mathrm{EKE} = \frac{(u')^2 + (v')^2}{2} \tag{7}$$

where u' and v' are the zonal and meridional components of the velocity anomaly (i.e. deviation from the mean flow). We use the Sea Surface Height Anomaly (SSHA), rather than the full SSH, to compute geostrophic and cyclogeostrophic velocity anomalies in the same manner as for total current velocity.

3.2.2 Evaluation against drifters

To validate that cyclogeostrophy provides a better estimate of surface currents than geostrophy, we compute evaluation metrics using drifter-derived velocities.

For each drifter observation i at time t_i and position $\mathbf{X}_i$, we define the inversion error for method M as:

$$\epsilon_M^{(i)} = \|\mathbf{u}_M(t_i, \mathbf{X}_i) - \mathbf{u}_d^{(i)}\| \tag{8}$$

where $\mathbf{u}_d$ is the drifter velocity vector and $\mathbf{u}_M$ is the velocity field obtained from the cyclogeostrophic ($M = cg$) or geostrophic ($M = g$) inversion, interpolated at the drifter time and position. Individual errors are binned into 1° latitude × 1° longitude boxes (Fig. C1 shows the number of observations per bin). Within each bin we compute the bias of an inversion method M using the mean inversion error:

$$\overline{\epsilon_M} = \frac{1}{N} \sum_{j=1}^{N} \epsilon_M^{(j)} \tag{9}$$

https://doi.org/10.5194/egusphere-2025-4172
Preprint. Discussion started: 4 September 2025

where N is the number of errors within the bin. We evaluate the robustness of an inversion method M by computing the standard error within each bin:

$$\hat{\sigma}_M = \sqrt{\frac{1}{N}\sum_{j=1}^{N}\left(\epsilon_M^{(j)} - \overline{\epsilon_M}\right)^2} \tag{10}$$

To compare error variability between two inversion methods, we use the normalized difference between their binned standard errors, defined as:

$$\widehat{\Delta\sigma}_{M_1-M_2} = 100\frac{\hat{\sigma}_{M_1} - \hat{\sigma}_{M_2}}{\hat{\sigma}_{M_1}} \tag{11}$$

This indicator quantifies the change in reliability of surface current estimates from SSH when using inversion method M_2 instead of M_1.

In addition to spatial binning, we also compute $\overline{\epsilon_M}$ and $\hat{\sigma}_M$ across bins defined around cyclogeostrophic EKE percentiles, as illustrated in Fig. 5.

4 Application to global maps of SSH

In this section, we apply the proposed cyclogeostrophic inversion method to global maps of SSH. We first analyze the resulting geostrophic and cyclogeostrophic surface currents, highlighting differences in dynamic regions. We then evaluate the reconstructed currents against independent drifter observations from the GDP to quantify improvements in accuracy. Unless otherwise specified, the cyclogeostrophic inversion method referred to throughout this section is the variational one.

4.1 Analysis of geostrophic and cyclogeostrophic currents

Surface currents derived from SSH using the geostrophic approximation and both variational and iterative cyclogeostrophic inversion methods are here qualitatively analyzed (i) with the cyclogeostrophic imbalance from Eq. 5, (ii) by observing the velocity and relative vorticity fields, and (iii) through a comparison of EKE.

The measure of the deviation from cyclogeostrophy shows that (i) geostrophy can be a coarse approximation of cyclogeostrophy at some location in space and time and (ii) the variational inversion method is more accurate than the iterative method to compute a cyclogeostrophic velocity field. These conclusions are drawn from the examination of Fig. 1 which presents the time-aggregated deviation from the cyclogeostrophic balance of 3 velocity fields derived from NeurOST SSH, namely the geostrophic field (top) and the cyclogeostrophic solutions from the variational method (bottom left) and the iterative method (bottom right). The geostrophic field exhibits large deviations from cyclogeostrophy, exceeding 0.3 ms^{-1} at nearly 5 % of grid points, hinting that the advection term should not be neglected. The solution of the iterative method deviates from cyclogeostrophy by 0.35 ms^{-1} at over 5 % of grid points, while the variational method shows deviations below 0.03 ms^{-1} at fewer than 5 % of points. This suggests that the iterative method is less reliable in converging toward a cyclogeostrophic solution, particularly

https://doi.org/10.5194/egusphere-2025-4172
Preprint. Discussion started: 4 September 2025

in the western boundary currents and the Agulhas current, where the variational method shows that a cyclogeostrophic solution exists.

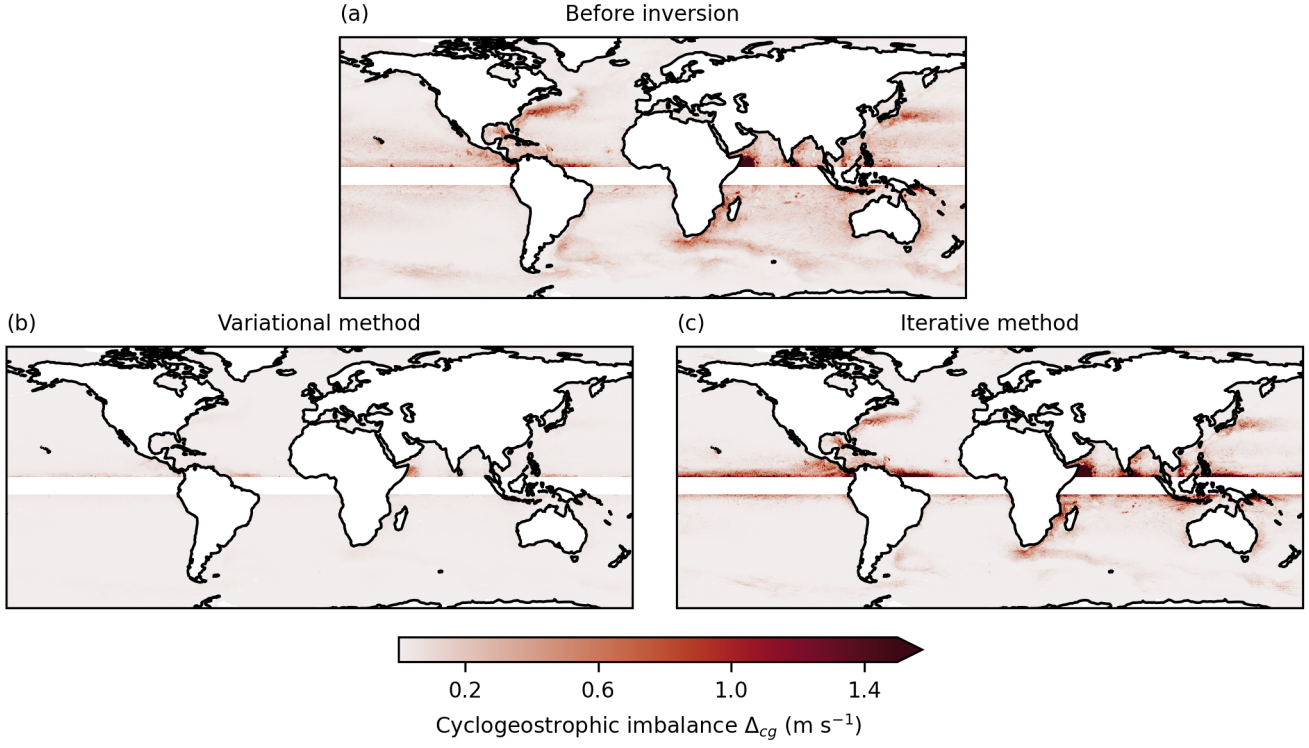

Figure 1. Maps of deviation from cyclogeostrophy, computed from Eq. 5, for the geostrophic velocity (a), the variational cyclogeostrophic velocity (b), and the iterative cyclogeostrophic velocity (c) derived from NeurOST SSH.

Our implementation of the proposed variational method enables physically consistent estimation of cyclogeostrophic currents on a global scale, including in highly dynamic regions where cyclogeostrophic corrections substantially impact jets and eddies, and where the iterative method yields unrealistic physical fields. Figure 2 presents a global snapshot of the norm of cyclogeostrophic currents derived from NeurOST SSH, along with a zoom on the Gulf Stream region where relative vorticity and differences compared to geostrophy are also displayed. In the northern (southern) branches of the Gulf Stream jet, positive (negative) cyclogeostrophic corrections reach up to ± 0.2 ms^{-1}. Similarly, anticyclonic (cyclonic) eddies exhibit cyclogeostrophic contributions of approximately $+0.2$ (-0.2) ms^{-1}, corresponding to differences from ± 10 % to ± 50 %. Finally, while the variational method allows for the reconstruction of a smooth and physically coherent relative vorticity field, the iterative method introduces artifacts in the most dynamic parts of the jet and eddies.

The EKE computed from the geostrophic and the variational cyclogeostrophic velocities anomalies exhibit differences up to 20 %, essentially at low and middle latitudes. This is shown in Figure 3, which presents the relative difference in EKE between cyclogeostrophy and geostrophy, averaged over the whole time period. Positive differences are particularly pronounced near

https://doi.org/10.5194/egusphere-2025-4172
Preprint. Discussion started: 4 September 2025

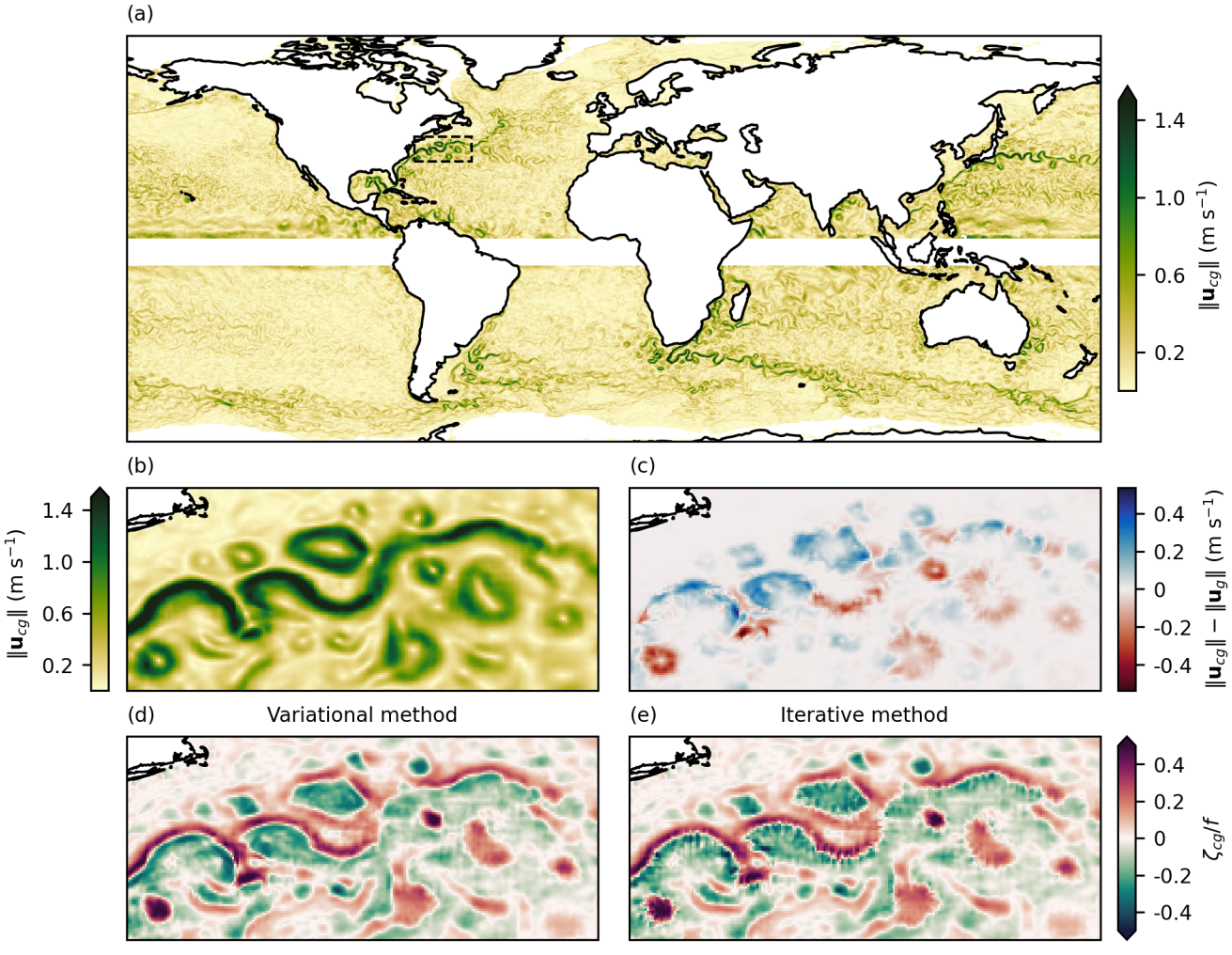

Figure 2. 16 April 2015 snapshots derived from NeurOST SSH. (a) Norm of the variational cyclogeostrophic velocity. (b) Same as (a), zoomed in the Gulf Stream region. (c) Difference between the norms of variational cyclogeostrophic and geostrophic velocities. (d) Relative vorticity computed from the variational cyclogeostrophic velocity. (e) Same as (d), using the iterative cyclogeostrophic velocity.

https://doi.org/10.5194/egusphere-2025-4172
Preprint. Discussion started: 4 September 2025

the equatorial band. Regions with intense dynamics such as the western boundary currents and the Agulhas current are characterized by elongated dipole structures with both positive and negative differences. These reflect a current intensification in anticyclonic eddies detaching poleward and a damping of the current in cyclonic eddies detaching equatorward, in agreement with the magnitude and sign of cyclogeostrophic corrections observed in Figure 2. All these observations are consistent with Cao et al. (2023) who performed a similar analysis with 1/4° DUACS maps and the historical iterative method for cyclogeostrophy over the period 1993-2018. Our results suggests once more that geostrophy can be a crude approximation leading to errors up to 20 % in EKE.

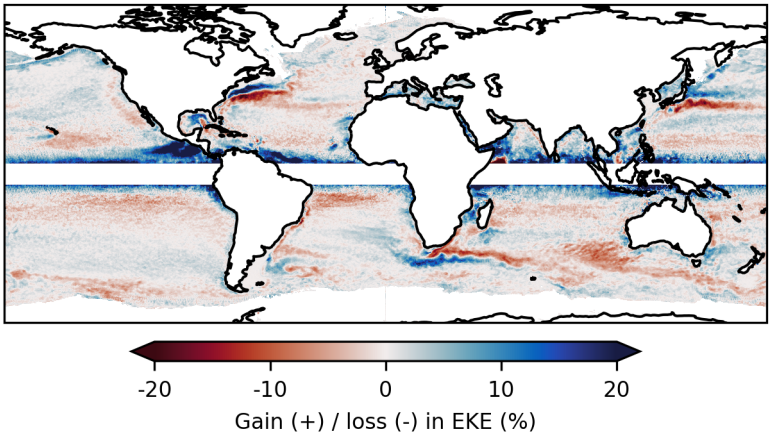

Figure 3. Relative difference in EKE between variational cyclogeostrophic and geostrophic current velocity anomalies derived from NeurOST SSH.

4.2 Evaluation with data from the GDP

Reconstructed cyclogeostrophic and geostrophic currents are evaluated against drifter-derived velocities using the binned standard error, as defined in Eq. 10, computed (i) within 1° latitude × 1° longitude boxes at the global scale and (ii) across EKE percentiles.

When using NeurOST SSH, variational cyclogeostrophic corrections improve surface current estimates, particularly in energetic regions such as western boundary currents and the Agulhas current, where reconstruction uncertainties are highest. This is illustrated in Figures 4 and 5. Fig. 4 presents global maps of the cyclogeostrophic standard error obtained from NeurOST SSH (top-left panel) and of the comparison between cyclogeostrophic and geostrophic inversion methods for NeurOST (top-right). Cyclogeostrophic standard error remains below 0.1 ms^{-1} across most of the ocean but increases to 0.2—0.5 ms^{-1} in energetic currents. In these regions, NeurOST-based cyclogeostrophy clearly reduces standard error, with improvements of up to 10 % in the Gulf Stream and over 20 % in the Kuroshio. Fig. 5 further illustrates this, showing the reconstruction bias and standard error for both geostrophy (blue bars) and cyclogeostrophy (green and red bars) around EKE percentiles. Focusing on

https://doi.org/10.5194/egusphere-2025-4172
Preprint. Discussion started: 4 September 2025

NeurOST-derived currents (solid bars), we find that at the highest EKE percentiles, cyclogeostrophy reduces reconstruction uncertainty by nearly 10 % upon geostrophy when employing the variational method, and by less than 5 % with the iterative method.

In contrast, cyclogeostrophic corrections can degrade performances when applied to DUACS SSH. This is again illustrated in Figures 4 and 5. The bottom-left panel of Fig. 4 compares cyclogeostrophic and geostrophic inversion methods based on DUACS SSH. Unlike results obtained with NeurOST, regions such as the western boundary currents and the Agulhas current show a degradation in performance of around 10 % when cyclogeostrophic corrections are applied. Similarly, the dashed bars in Fig. 5 show the standard error across EKE percentiles for DUACS-based surface currents using the variational method (green), the iterative method (red), and geostrophy (blue). Across all EKE percentiles, the three methods perform similarly, with cyclogeostrophic approaches showing a slight deterioration in performance as EKE increases. These discrepancies could stem from differences in the effective resolution of the SSH products: DUACS may insufficiently capture fine-scale structures, deteriorating the accuracy of cyclogeostrophic correction in energetic regions.

Importantly, the combination of higher effective resolution SSH fields and cyclogeostrophic inversion yields substantial benefits over the current operational standard. As shown in Fig. 4 (bottom-right panel), applying variational cyclogeostrophy to NeurOST SSH reduces reconstruction standard error by 5—20 % at mid-latitudes relative to DUACS geostrophy. Fig. 5 confirms this result across EKE percentiles: NeurOST-based variational cyclogeostrophy (green, solid bar) yields an 8 % reduction in standard error at low EKE (0.05 $\mathrm{m^2 s^{-2}}$), and up to 15 % at higher EKE (0.35 $\mathrm{m^2 s^{-2}}$) compared to DUACS geostrophy (blue, dashed bar). These results suggest that cyclogeostrophic corrections will become increasingly relevant as SSH products achieve higher effective resolution and could significantly benefit future operational surface current products.

5 Discussion and conclusions

We developed a new and robust method for the cyclogeostrophic inversion of surface currents by reformulating the inversion problem in a variational framework, thereby overcoming the limitations of the traditional iterative approach. The method is implemented as an open-source Python package, `jaxparrow`, which leverages the JAX library for high-performance and scalable computation, enabling its application at the global scale. When applied to NeurOST SSH fields, the proposed approach yields physically consistent cyclogeostrophic current estimates, particularly in energetic regions. The relevance of the cyclogeostrophic corrections derived with our variational method is supported by a global, 13-year comparison with drifter-derived velocities.

This work makes systematic application of cyclogeostrophic inversion feasible, providing a complementary tool for surface current reconstruction from operational SSH products.

Several questions were not addressed in this study. By formulating the cost functional J from Eq. 4 as a domain integral, the solution to the minimization problem depends on the entire study region. Moreover, we did not investigate the sensitivity of the minimization solution to the choice of the optimizer and its hyperparameters. These points suggest potential avenues for investigation, such as partitioning the domain into sub-regions and applying different minimization strategies tailored to the en-

https://doi.org/10.5194/egusphere-2025-4172
Preprint. Discussion started: 4 September 2025

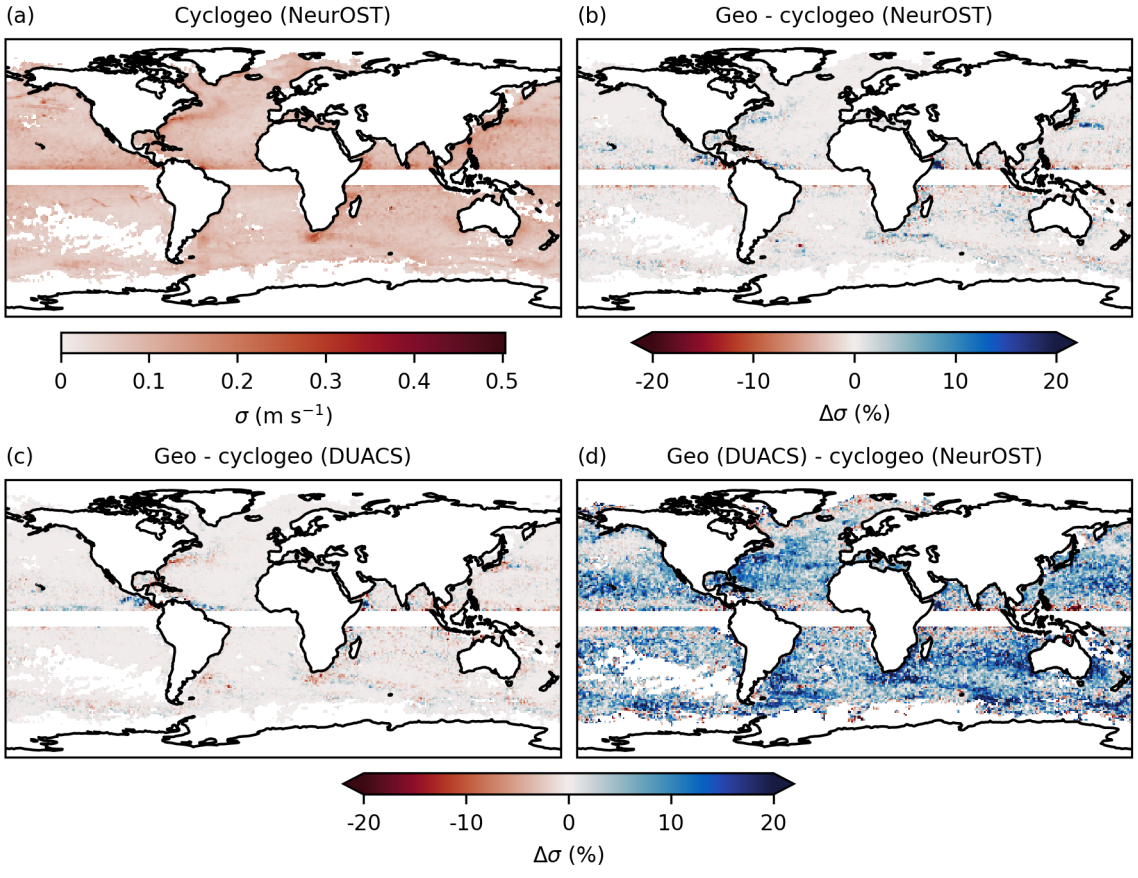

Figure 4. (a) Standard errors with respect to the drifters for the cyclogeostrophic velocity estimated from NeurOST SSH. (b) Relative difference of NeurOST-derived geostrophic and cyclogeostrophic velocities standard errors. (c) Same as (b) but using SSH from DUACS. (d) Same as (b) but between DUACS geostrophic velocities and NeurOST cyclogeostrophic velocities. See Fig. C2 for the corresponding plot of the bias instead of the standard error.

https://doi.org/10.5194/egusphere-2025-4172
Preprint. Discussion started: 4 September 2025

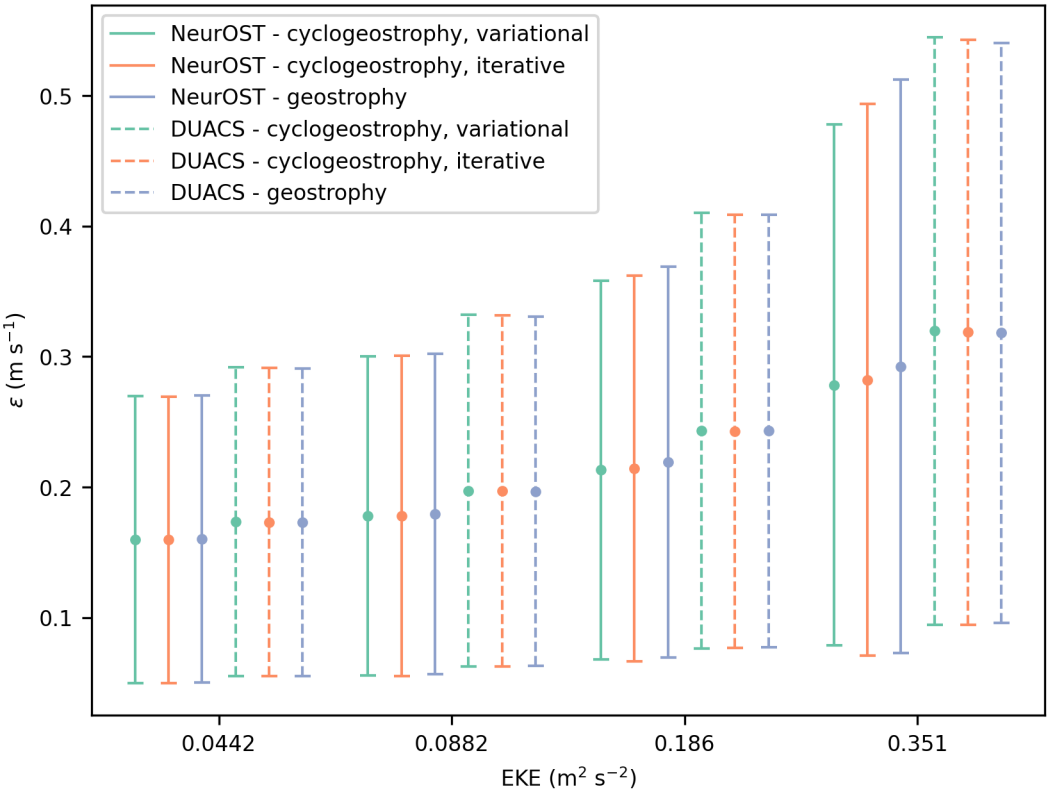

Figure 5. Bias and standard error with respect to the drifters around EKE percentiles. Solid error bars refer to NeurOST-derived velocities and dashed error bars to DUACS-derived velocities ; green refers to variational cyclogeostrophic velocities, red to iterative cyclogeostrophic velocities, and blue to geostrophic velocities.

ergetic conditions of each area. Furthermore, drifter-based validation does not fully isolate the geostrophic or cyclogeostrophic components of motion, and to our knowledge there is no well established processing (i.e. filtering) of drifter-derived velocities designed for geostrophic or cyclogeostrophic currents evaluation.

In addition to enabling the inclusion of cyclogeostrophic corrections in operational SSH and surface current products, our work opens several new opportunities. With its effective resolution reaching 15 km within the swath, the SWOT mission offers unprecedented possibilities for observing and studying the submesoscales. While several efforts are currently underway to accurately separate balanced and unbalanced signals from SWOT SSH (Gao et al., 2024; Tranchant et al., 2025), our implementation provides a practical approach for reconstructing cyclogeostrophic currents and thus extending SSH-based diagnostics beyond the geostrophic approximation, as illustrated in Fig. B1. Furthermore, the development of Data Assimilation (DA) systems for General Circulation Models (GCMs) or Ocean GCMs (OGCMs) typically requires building and maintaining their tangent linear and adjoint models—a complex and time-consuming task. Recent progress in differentiable programming frameworks such as JAX and Julia (Bezanson et al., 2017) now allows for automatic differentiation of GCMs, enabling direct

https://doi.org/10.5194/egusphere-2025-4172
Preprint. Discussion started: 4 September 2025

access to their tangent linear and adjoint models (Kochkov et al., 2024; Häfner et al., 2018). As our cyclogeostrophic inversion method is fully implemented in JAX, it can be readily integrated as a modular component into such DA systems.

Code and data availability. The DUACS delayed-time altimeter gridded maps of sea surface height product used in this study is freely available on the CMEMS portal: https://doi.org/10.48670/moi-00148.

The NeurOST delayed-time altimeter gridded maps of sea surface height product used in this study is freely available on the PO.DAAC portal: https://doi.org/10.5067/NEURO-STV24.

The six-hourly interpolated drifters data used in this study is freely available on the NOAA portal: https://doi.org/10.25921/7ntx-z961, or via the `clouddrift` Python library: https://doi.org/10.5281/zenodo.11081647.

The subset data of the eNATL60-BLB002 simulation is available on Zenodo: https://doi.org/10.5281/zenodo.16099419.

The SWOT L3 Expert data in its version v2_0_1 is available through the AVISO+ portal: https://doi.org/10.24400/527896/A01-2023.018.

All the diagnostics computed and used in this study are available on Zenodo: https://doi.org/10.5281/zenodo.16099419.

The code used to run this study experiments and produce the diagnostics presented here (including the appendices) can be found on GitHub: https://github.com/vadmbertr/cyclogeostrophy_impact_experiment.

The code of the Python library `jaxparrow` introduced in this paper is also available on GitHub: https://github.com/meom-group/jaxparrow.

https://doi.org/10.5194/egusphere-2025-4172
Preprint. Discussion started: 4 September 2025

Appendix A: Variational cyclogeostrophic inversion from NEMO-eNATL60 SSH

As a qualitative assessment of the benefit of the variational method for the inversion of cyclogeostrophic currents we present snapshots obtained from eNATL60-BLB002 (no tides) (Brodeau et al., 2020) simulation based on NEMO. This simulation covers the North Atlantic, plus the Mediterranean Sea, with a 1/60° horizontal resolution. We choose snapshots of the Alboran Sea as it features two large and persistent gyres subject to cyclogeostrophy.

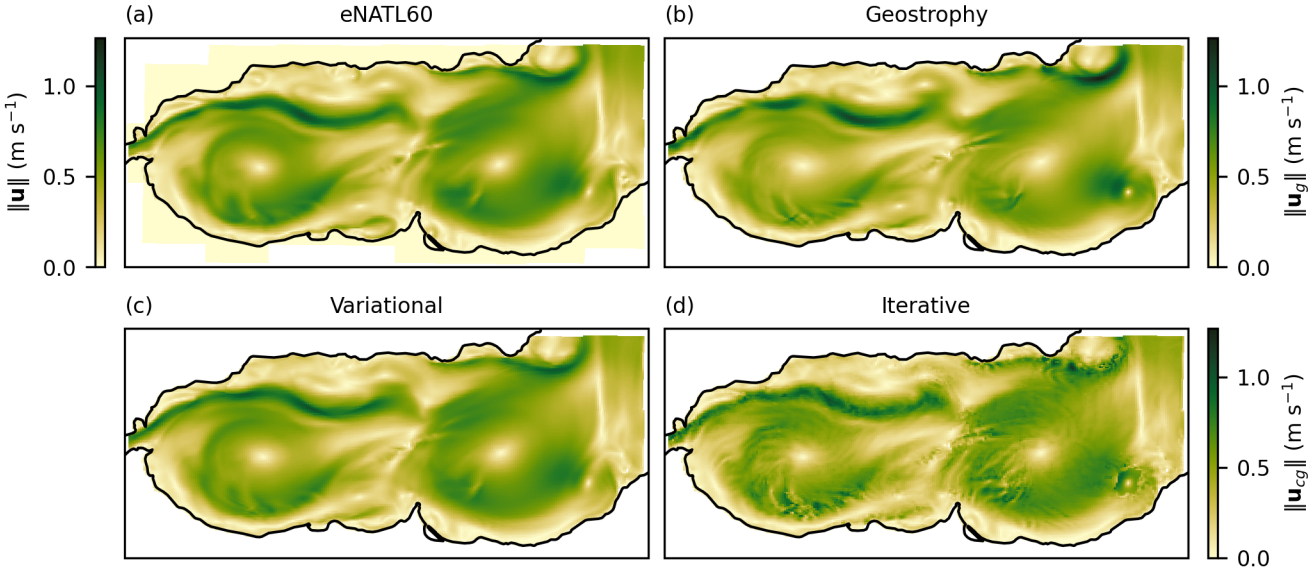

Figure A1. 1 July 2009 at 00:30:00 snapshots derived from eNATL60-BLB002 (no tides). (a) Norm of the simulation currents. (b) Norm of the geostrophic currents derived from the SSH. (c) Norm of the cyclogeostrophic currents derived from the SSH using the variational method. (d) Same as (c), using the iterative method.

https://doi.org/10.5194/egusphere-2025-4172
Preprint. Discussion started: 4 September 2025

Appendix B: Variational cyclogeostrophic inversion in the SWOT swath

To illustrate the use of our implementation of the variational cyclogeostrophic inversion on irregular grids we show inversion results in the SWOT swath. We use the SWOT L3 Expert data in its version v2_0_1. This product has a spatial resolution of 2 km. We computed the SSH used for the inversion as the sum of the MDT and SSHA_Filtered variables of the dataset. Readers interesting in a demonstration of how to apply the cyclogeostrophic inversion to L3 SWOT SSH maps can refer to the notebook `appendix-figures.ipynb` available in the GitHub repository at https://github.com/vadmbertr/cyclogeostrophy_impact_experiment, under the `paper-results-reproduction` directory.

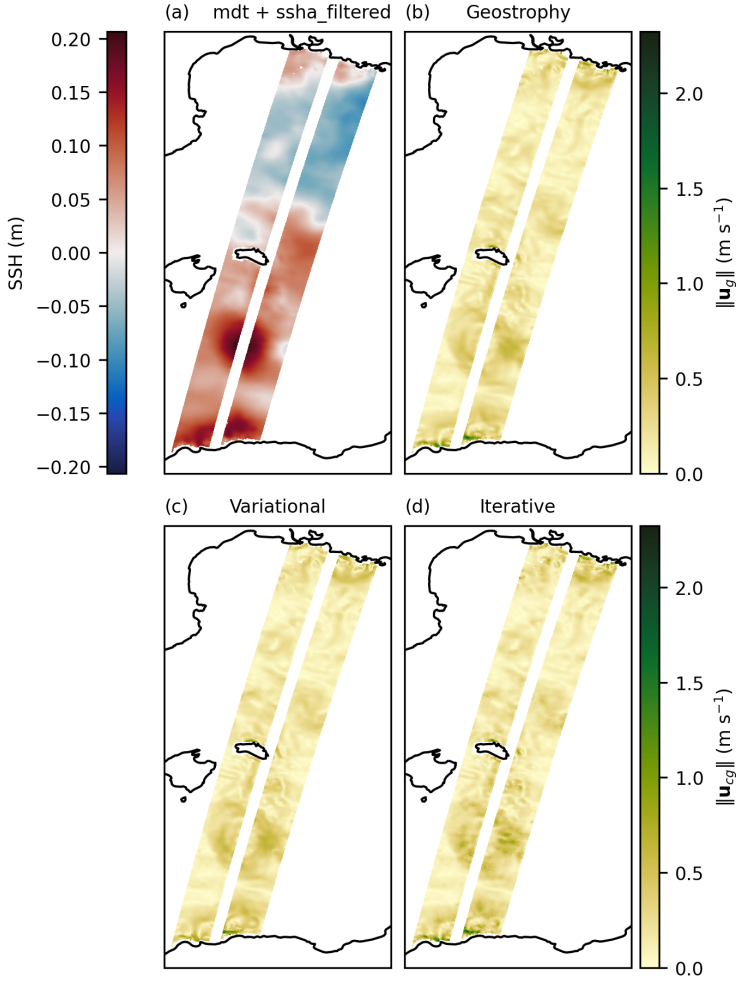

Figure B1. 8 June 2023 snapshots derived from SWOT L3 SSH. (a) SSH = MDT + SSHA_Filtered. (b) Norm of the geostrophic currents derived from the SSH. (c) Norm of the cyclogeostrophic currents derived from the SSH using the variational method. (d) Same as (c), using the iterative method.

https://doi.org/10.5194/egusphere-2025-4172
Preprint. Discussion started: 4 September 2025

Appendix C: Evaluation with data from the GDP

This section provides additional plots supporting our evaluation of the reconstructed currents using data from the GDP.

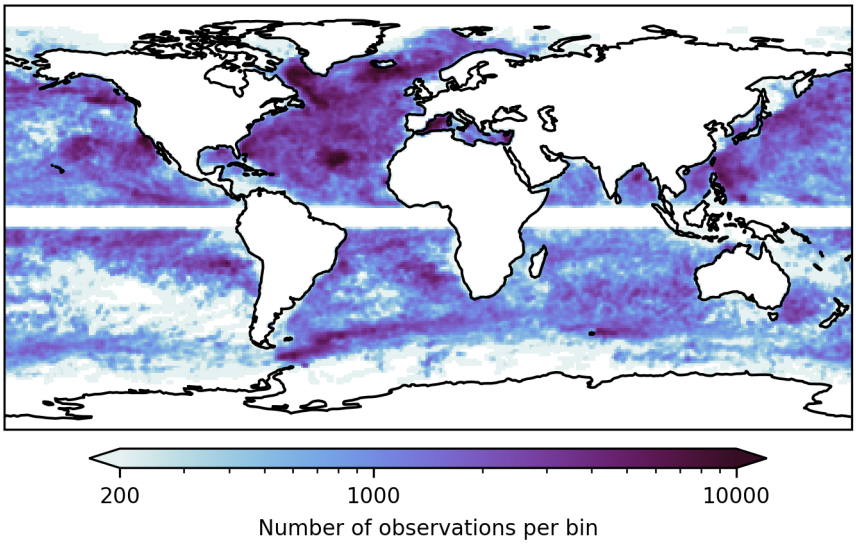

Figure C1. Number of drifter observations per 1° latitude × 1° longitude bin.

https://doi.org/10.5194/egusphere-2025-4172
Preprint. Discussion started: 4 September 2025

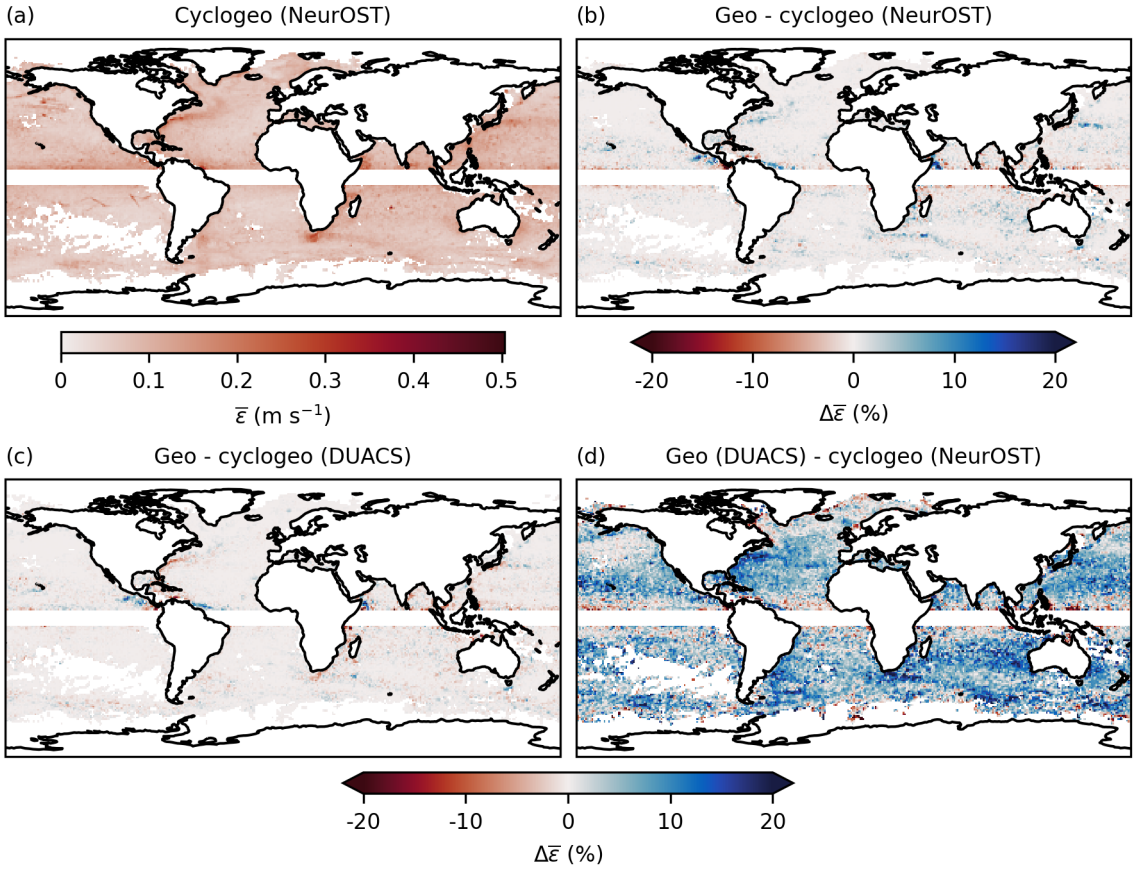

Figure C2. Same as Fig. 4, but using the mean instead of the standard deviation for spatial binning.

Author contributions. VB developed the Python package `jaxparrow`, designed and ran the experiments and analysis, and wrote the manuscript. EC proposed the variational cyclogeostrophic inversion formulation. VZDA carried out the initial work on the implementation in JAX of the variational cyclogeostrophic inversion. JLS and EC contributed to the design of the experiments, and the writing of the manuscript. JLS, AS and EC contributed to the analysis. JLS and EC acquired funding. All authors reviewed the manuscript.

Competing interests. No competing interests are present.

Acknowledgements. This research was funded by the French National Space Agency (CNES) through the SWOT Science Team program (SWOT-MIDAS project); by the European Union's Horizon Europe research and innovation programme under the grant No 101093293

https://doi.org/10.5194/egusphere-2025-4172
Preprint. Discussion started: 4 September 2025

(EDITO-Model Lab project). The authors would like to thank Maxime Ballarotta, Sammy Metref, and Clément Ubelmann for their feedback on the draft version of this paper.

https://doi.org/10.5194/egusphere-2025-4172
Preprint. Discussion started: 4 September 2025

References

Archambault, T., Filoche, A., Charantonis, A. A., and Béréziat, D.: Multimodal Unsupervised Spatio-Temporal Interpolation of Satellite Ocean Altimetry Maps, https://hal.sorbonne-universite.fr/hal-03934647, 2023.

Arnason, G., Haltiner, G. J., and Frawley, M. J.: Higher-order geostrophic wind approximations, Monthly Weather Review, pp. 175–195, 1962.

Ballarotta, M., Ubelmann, C., Pujol, M.-I., Taburet, G., Fournier, F., Legeais, J.-F., Faugère, Y., Delepoulle, A., Chelton, D., Dibarboure, G., and Picot, N.: On the Resolutions of Ocean Altimetry Maps, Ocean Science, 15, 1091–1109, https://doi.org/10.5194/os-15-1091-2019, 2019.

Ballarotta, M., Ubelmann, C., Veillard, P., Prandi, P., Etienne, H., Mulet, S., Faugère, Y., Dibarboure, G., Morrow, R., and Picot, N.: Improved global sea surface height and current maps from remote sensing and in situ observations, Earth System Science Data, 15, 295–315, https://doi.org/10.5194/essd-15-295-2023, 2023.

Bertrand, V., E V Z De Almeida, V., Le Sommer, J., and Cosme, E.: jaxparrow, https://doi.org/10.5281/zenodo.13886070, 2025.

Bezanson, J., Edelman, A., Karpinski, S., and Shah, V. B.: Julia: A fresh approach to numerical computing, SIAM Review, 59, 65–98, https://doi.org/10.1137/141000671, 2017.

Bradbury, J., Frostig, R., Hawkins, P., Johnson, M. J., Leary, C., Maclaurin, D., Necula, G., Paszke, A., VanderPlas, J., Wanderman-Milne, S., and Zhang, Q.: JAX: composable transformations of Python+NumPy programs, http://github.com/jax-ml/jax, 2018.

Breivik, O., Allen, A. A., Maisondieu, C., and Olagnon, M.: Advances in Search and Rescue at Sea, Ocean Dynamics, 63, 83–88, https://doi.org/10.1007/s10236-012-0581-1, 2013.

Brodeau, L., Sommer, J. L., and Albert, A.: Ocean-next/eNATL60: Material Describing the Set-up and the Assessment of NEMO-eNATL60 Simulations, Zenodo, https://doi.org/10.5281/zenodo.4032732, 2020.

Buongiorno Nardelli, B., Cavaliere, D., Charles, E., and Ciani, D.: Super-Resolving Ocean Dynamics from Space with Computer Vision Algorithms, Remote Sensing, 14, 1159, https://doi.org/10.3390/rs14051159, 2022.

Cao, Y., Dong, C., Stegner, A., Bethel, B. J., Li, C., Dong, J., Lü, H., and Yang, J.: Global Sea Surface Cyclogeostrophic Currents Derived From Satellite Altimetry Data, Journal of Geophysical Research: Oceans, 128, e2022JC019 357, https://doi.org/10.1029/2022JC019357, 2023.

De Dominicis, M., Bruciaferri, D., Gerin, R., Pinardi, N., Poulain, P., Garreau, P., Zodiatis, G., Perivoliotis, L., Fazioli, L., Sorgente, R., and Manganiello, C.: A multi-model assessment of the impact of currents, waves and wind in modelling surface drifters and oil spill, Deep Sea Research Part II: Topical Studies in Oceanography, 133, 21–38, https://doi.org/https://doi.org/10.1016/j.dsr2.2016.04.002, 2016.

DeepMind, Babuschkin, I., Baumli, K., Bell, A., Bhupatiraju, S., Bruce, J., Buchlovsky, P., Budden, D., Cai, T., Clark, A., Danihelka, I., Dedieu, A., Fantacci, C., Godwin, J., Jones, C., Hemsley, R., Hennigan, T., Hessel, M., Hou, S., Kapturowski, S., Keck, T., Kemaev, I., King, M., Kunesch, M., Martens, L., Merzic, H., Mikulik, V., Norman, T., Papamakarios, G., Quan, J., Ring, R., Ruiz, F., Sanchez, A., Sartran, L., Schneider, R., Sezener, E., Spencer, S., Srinivasan, S., Stanojević, M., Stokowiec, W., Wang, L., Zhou, G., and Viola, F.: The DeepMind JAX Ecosystem, http://github.com/google-deepmind, 2020.

DUACS: Global Ocean Gridded L 4 Sea Surface Heights And Derived Variables Reprocessed 1993 Ongoing, https://doi.org/10.48670/moi-00148, 2024.

Endlich, R. M.: Computation and uses of gradient winds, Monthly Weather Review, pp. 187–191, 1961.

https://doi.org/10.5194/egusphere-2025-4172
Preprint. Discussion started: 4 September 2025

Fablet, R., Chapron, B., Le Sommer, J., and Sévellec, F.: Inversion of Sea Surface Currents From Satellite-Derived SST-SSH Synergies With 4DVarNets, Journal of Advances in Modeling Earth Systems, 16, e2023MS003 609, https://doi.org/10.1029/2023MS003609, 2024.

Ferreira, R. M., Estefen, S. F., and Romeiser, R.: Under What Conditions SAR Along-Track Interferometry is Suitable for Assessment of Tidal Energy Resource, IEEE Journal of Selected Topics in Applied Earth Observations and Remote Sensing, 9, 5011–5022, https://doi.org/10.1109/JSTARS.2016.2581188, 2016.

Fu, L., Rodriguez, E., Alsdorf, D., and Morrow, R.: The SWOT Mission Science document, Tech. rep., NASA/JPL, 2012.

Fu, L.-L.: Observing Oceanic Submesoscale Processes From Space, Eos, Transactions, American Geophysical Union (EOS), 89, 488–489, 2008.

Gao, Z., Chapron, B., Ma, C., Fablet, R., Febvre, Q., Zhao, W., and Chen, G.: A Deep Learning Approach to Extract Balanced Motions From Sea Surface Height Snapshot, Geophysical Research Letters, 51, e2023GL106 623, https://doi.org/10.1029/2023GL106623, 2024.

Häfner, D., Løwe Jacobsen, R., Eden, C., Kristensen, M. R. B., Jochum, M., Nuterman, R., and Vinter, B.: A Fast Versatile Ocean Simulator (Veros) in Pure Python, in: EGU General Assembly Conference Abstracts, p. 7122, 2018.

Hewitt, H., Fox-Kemper, B., Pearson, B., Roberts, M., and Klocke, D.: The small scales of the ocean may hold the key to surprises, Nature Climate Change, 12, 496–499, https://doi.org/10.1038/s41558-022-01386-6, 2022.

Ioannou, A., Stegner, A., Tuel, A., LeVu, B., Dumas, F., and Speich, S.: Cyclostrophic Corrections of AVISO/DUACS Surface Velocities and Its Application to Mesoscale Eddies in the Mediterranean Sea, Journal of Geophysical Research: Oceans, 124, 8913–8932, https://doi.org/10.1029/2019JC015031, 2019.

Keghouche, I., Bertino, L., and Lisæter, K.: Parameterization of an Iceberg Drift Model in the Barents Sea, Journal of Atmospheric and Oceanic Technology - J ATMOS OCEAN TECHNOL, 26, https://doi.org/10.1175/2009JTECHO678.1, 2009.

Kochkov, D., Yuval, J., Langmore, I., Norgaard, P., Smith, J., Mooers, G., Klöwer, M., Lottes, J., Rasp, S., Düben, P., Hatfield, S., Battaglia, P., Sanchez-Gonzalez, A., Willson, M., Brenner, M. P., and Hoyer, S.: Neural General Circulation Models for Weather and Climate, Nature, 632, 1060–1066, https://doi.org/10.1038/s41586-024-07744-y, 2024.

Le Guillou, F., Metref, S., Cosme, E., Ubelmann, M., Ballarotta, M., Sommer, J. L., and Verron, J.: Mapping Altimetry in the Forthcoming SWOT Era by Back-and-Forth Nudging a One-Layer Quasigeostrophic Model, JOURNAL OF ATMOSPHERIC AND OCEANIC TECHNOLOGY, 38, 2021.

Le Guillou, F., Gaultier, L., Ballarotta, M., Metref, S., Ubelmann, C., Cosme, E., and Rio, M.-H.: Regional mapping of energetic short mesoscale ocean dynamics from altimetry: performances from real observations., EGUsphere, 2023, 1–17, https://doi.org/10.5194/egusphere-2023-509, 2023.

Le Guillou, F., Chapron, B., and Rio, M.-H.: VarDyn: Dynamical joint-reconstructions of Sea Surface Height and Temperature from multi-sensor satellite observations, submitted to Journal of Advances in Modeling Earth Systems (JAMES), https://doi.org/10.22541/essoar.172616118.81277809/v1, 2024.

Le Traon, P.-Y. and Dibarboure, G.: Mesoscale Mapping Capabilities of Multiple-Satellite Altimeter Missions, J. Atmos. Ocean. Tech., 16, 1208–1223, 1999.

Le Traon, P.-Y. and Dibarboure, G.: Velocity Mapping Capabilities of Present and Future Altimeter Missions: The Role of High-Frequency Signals, J. Atmos. Ocean. Tech., 19, 2077–2087, 2002.

Lumpkin, R. and Centurioni, L.: Global Drifter Program quality-controlled 6-hour interpolated data from ocean surface drifting buoys. [2020-2022]. NOAA National Centers for Environmental Information. Dataset. Accessed [March 2024]., https://doi.org/10.25921/7ntx-z961, 2019.

https://doi.org/10.5194/egusphere-2025-4172
Preprint. Discussion started: 4 September 2025

Lévy, M., Franks, P. J. S., and Smith, K. S.: The role of submesoscale currents in structuring marine ecosystems, Nature Communications, 9, 4758, https://doi.org/10.1038/s41467-018-07059-3, 2018.

Mahadevan, A.: The Impact of Submesoscale Physics on Primary Productivity of Plankton, Annual Review of Marine Science, 8, 161–184, https://doi.org/10.1146/annurev-marine-010814-015912, 2016.

Martin, S. A., Manucharyan, G. E., and Klein, P.: Deep Learning Improves Global Satellite Observations of Ocean Eddy Dynamics, Geophysical Research Letters, 51, e2024GL110 059, https://doi.org/10.1029/2024GL110059, 2024.

McWilliams, J. C.: A survey of submesoscale currents, Geoscience Letters, 6, 3, https://doi.org/10.1186/s40562-019-0133-3, 2019.

Morrow, R., Fu, L.-L., Ardhuin, F., Benkiran, M., Chapron, B., Cosme, E., d'Ovidio, F., Farrar, J. T., Gille, S. T., Lapeyre, G., Le Traon, P.-Y., Pascual, A., Ponte, A., Qiu, B., Rascle, N., Ubelmann, C., Wang, J., and Zaron, E. D.: Global Observations of Fine-Scale Ocean Surface Topography With the Surface Water and Ocean Topography (SWOT) Mission, Frontiers in Marine Science, 6, 232, https://doi.org/10.3389/fmars.2019.00232, 2019.

Nencioli, F., Raynal, M., Ubelmann, C., Cadier, E., Prandi, P., and Dibarboure, G.: An Altimeter-Based Assessment of SWOT KaRIn Spectral Error Requirements, Advances in Space Research, 76, 1241–1261, https://doi.org/10.1016/j.asr.2025.05.073, 2025.

NeurOST: Daily NeurOST L4 Sea Surface Height and Surface Geostrophic Currents, https://doi.org/10.5067/NEURO-STV24, 2024.

Penven, P., Halo, I., Pous, S., and Marié, L.: Cyclogeostrophic balance inthe Mozambique Channel, J. Geophys. Res. Oceans, 119, 2014.

Röhrs, J., Sutherland, G., Jeans, G., Bedington, M., Sperrevik, A. K., Dagestad, K.-F., Gusdal, Y., Mauritzen, C., Dale, A., and LaCasce, J. H.: Surface Currents in Operational Oceanography: Key Applications, Mechanisms, and Methods, Journal of Operational Oceanography, 16, 60–88, https://doi.org/10.1080/1755876X.2021.1903221, 2023.

Taburet, G., Sanchez-Roman, A., Ballarotta, M., Pujol, M.-I., Legeais, J.-F., Fournier, F., Faugere, Y., and Dibarboure, G.: DUACS DT2018: 25 years of reprocessed sea level altimetry products, Ocean Science, 15, 1207–1224, https://doi.org/10.5194/os-15-1207-2019, 2019.

Taylor, J. R. and Thompson, A. F.: Submesoscale Dynamics in the Upper Ocean, Annual Review of Fluid Mechanics, 55, 103–127, https://doi.org/10.1146/annurev-fluid-031422-095147, 2023.

Tranchant, Y.-T., Legresy, B., Foppert, A., Pena-Molino, B., and Phillips, H. E.: SWOT Reveals Fine-Scale Balanced Motions and Dispersion Properties in the Antarctic Circumpolar Current, https://doi.org/10.22541/essoar.173655552.25945463/v1, 2025.

Trinanes, J. A., Olascoaga, M. J., Goni, G. J., Maximenko, N. A., Griffin, D. A., and Hafner, J.: Analysis of flight MH370 potential debris trajectories using ocean observations and numerical model results, Journal of Operational Oceanography, 9, 126–138, https://doi.org/10.1080/1755876X.2016.1248149, 2016.

Ubelmann, C., Dibarboure, G., Gaultier, L., Ponte, A., Ardhuin, F., Ballarotta, M., and Faugère, Y.: Reconstructing Ocean Surface Current Combining Altimetry and Future Spaceborne Doppler Data, Journal of Geophysical Research: Oceans, 126, e2020JC016 560, https://doi.org/10.1029/2020JC016560, 2021.

Wang, J., Lucas, A. J., Stalin, S., Lankhorst, M., Send, U., Schofield, O., Kachelein, L., Haines, B., Meinig, C., Pinkel, R., Farrar, J. T., and Fu, L.-L.: SWOT Mission Validation of Sea Surface Height Measurements at Sub-100 Km Scales, Geophysical Research Letters, 52, e2025GL114 936, https://doi.org/10.1029/2025GL114936, 2025.

Xiao, Q., Balwada, D., Jones, C. S., Herrero-González, M., Smith, K. S., and Abernathey, R.: Reconstruction of Surface Kinematics From Sea Surface Height Using Neural Networks, Journal of Advances in Modeling Earth Systems, 15, e2023MS003 709, https://doi.org/10.1029/2023MS003709, 2023.